Geomorphology 234 (2015) 64–79

Contents lists available at ScienceDirect

Geomorphology

journal homepage: www.elsevier.com/locate/geomorph

Sinkhole susceptibility mapping using the analytical hierarchy process (AHP) and magnitude–frequency relationships: A case study in Hamadan province, Iran

Kamal Taheri [a,1], Francisco Gutiérrez [b], Hassan Mohseni [c], Ezzat Raeisi [d], Milad Taheri [c]

[a] Islamic Azad University, Research and Sciences Branch, Tehran, Iran
[b] Earth Science Department, Edificio Geológicas, Universidad de Zaragoza, Zaragoza, Spain
[c] Department of Geology, Faculty of Sciences, Bu-Ali Sina University, Hamadan, Iran
[d] Department of Earth Sciences, College of Sciences, Shiraz University, Shiraz, Iran

ARTICLE INFO

Article history:
Received 17 May 2014
Received in revised form 3 January 2015
Accepted 14 January 2015
Available online 22 January 2015

Keywords:
Sinkhole susceptibility mapping
AHP
Groundwater over-exploitation
Karst
Iran

ABSTRACT

Since 1989, an increasing number of sinkhole occurrences have been reported in the Kabudar Ahang and Razan–Qahavand subcatchments (KRQ) of Hamadan province, western Iran. The sinkhole-related subsidence phenomenon poses a significant threat for people and human structures, including sensitive facilities like the Hamadan Power Plant. Groundwater over-exploitation from the thick alluvial cover and the underlying cavernous limestone has been identified as the main factor involved in sinkhole development. A sinkhole susceptibility model was produced in a GIS environment applying the analytical hierarchy process (AHP) approach and considering a selection of eight factors, each categorized into five classes: distance to faults (DF), water level decline (WLD), groundwater exploitation (GE), penetration of deep wells into karst bedrock (PKA), distance to deep wells (DDW), groundwater alkalinity (GA), bedrock lithology (BL), and alluvium thickness (AT). Relative weights were preliminarily assigned to each factor and to their different classes through systematic pairwise comparisons based on expert judgment. The resulting sinkhole susceptibility index (SSI) values were then classified into four susceptibility classes: low, moderate, high and very high susceptibility. Subsequently, the model was refined through a trial and error process involving changes in the relative weights and iterative evaluation of the prediction capability. Independent evaluation of the final model indicates that 55% and 45% of the subsidence events fall within the very high and high, susceptibility zones, respectively. The results of this study show that AHP can be a useful approach for susceptibility assessment if data on the main controlling factors have sufficient accuracy and spatial coverage. The limitations of the model are partly related to the difficulty of gathering data on some important geological factors, due to their hidden nature. The magnitude and frequency relationship constructed with the 41 sinkholes with chronological and morphometric data indicates maximum recurrence intervals of 1.17, 2.14 and 4.18 years for sinkholes with major axial lengths equal to or higher than 10 m, 20 m, and 30 m, respectively.

1. Introduction

During the last two decades, sinkholes have become a major concern in some regions of Iran due to the hazard increase, mainly induced by groundwater over-exploitation. “Forochaleh” is a Persian word used to designate sinkholes; enclosed depressions with internal drainage developed in karst terrains. In the Kurdish language, “barqe chal” means sudden collapse, whereas “noor” refers to karst sinkhole (Taheri and Hashemi, 2011). The term “doline” is mainly used by European geomorphologists, whereas sinkhole is the most common term in North America and in the international literature dealing with engineering and environmental issues associated with karst (Gunn, 2004; Gutiérrez et al., 2008a, 2014). Words like collapse and sinkhole are also used by some authors to designate depressions and holes generated by subsidence phenomena related to anthropogenic cavities like mines, dwellings, catacombs, and other underground excavations (e.g. Parise, 2012, 2013). In this work we follow the genetic sinkhole classification proposed by Gutiérrez et al. (2008b, 2014), which covers the whole range of subsidence mechanisms observed in both carbonate and evaporite karst.

Some of the main topics addressed in the scientific literature related to sinkholes include their nomenclature and classification (White, 1988; Waltham et al., 2005; Gutiérrez et al., 2008b), formation mechanisms (Tharp, 1999, 2002; Gutiérrez and Cooper, 2002; Salvati and Sasowsky, 2002; Karimi and Taheri, 2010; Heidari et al., 2011; Parise and Lollino,

E-mail addresses: Taheri.kamal@gmail.com (K. Taheri), fgutier@unizar.es (F. Gutiérrez), mohseni@basu.ac.ir (H. Mohseni), e_raeisi@yahoo.com (E. Raeisi), milad.thr@gmail.com (M. Taheri).
[1] Current address: Karst Research and Study Office of Western Iran, Kermanshah Regional Water Authority, Iran. Tel./fax: +98 831 8360005.

http://dx.doi.org/10.1016/j.geomorph.2015.01.005
0169-555X/

2011; Zhou and Beck, 2011; Shalev and Lyakhovsky, 2012), detrimental effects on human structures (Gutiérrez and Cooper, 2002; Fidelibus et al., 2011), role played on aquifer contamination (Lindsey et al., 2010), interaction with engineering projects and remediation (Waltham and Fookes, 2003; Milanović, 2004, 2011; Tolmachev and Leonenko, 2011; Galve et al., 2012a; Song et al., 2012). One of the issues that has received greater attention in recent years is the development of susceptibility and hazard maps aimed at predicting the spatial distribution, or spatial and temporal distribution of new sinkholes, respectively. These models may be produced through several approaches, like zonings delineated on the basis of expert judgments (Edmonds et al., 1987; Bruno et al., 2008; Kaufmann, 2008), the analysis of geophysical data (Batayneh, 2006; Pueyo-Anchuela et al., 2009; García-Moreno and Mateos, 2011; Margiotta et al., 2012), and data on peak ground acceleration (Papadopoulou-Vrynioti et al., 2013). Galve et al. (2008, 2009a,b, 2011, 2012b), in a series of papers, propose a complete methodological sequence for sinkhole susceptibility, hazard and risk assessment, as well as for the identification of suitable and cost-effective risk mitigation solutions. The main steps of the work flow, performed in a GIS environment, include: (1) development of multiple susceptibility models based on the distribution of inventoried sinkholes, on the one hand, and on the statistical relationships between the sinkholes and different sets of conditioning factors, on the other hand; (2) quantitative and independent evaluation of the prediction capability of the models and selection of the most reliable one; (3) transformation of the selected susceptibility model into a hazard model considering the temporal frequency of sinkholes in each susceptibility class, and incorporating a magnitude–frequency scaling relationship; (4) production of risk models combining the hazard model with data on the vulnerability of the human elements; and (5) assessment of the cost-effectiveness of different mitigation measures and layouts performing a cost–benefit analysis.

The sinkholes in the northern plains of Hamadan province, Iran, have been the focus of numerous studies, but most of them have been produced in Persian (Zamiran Consulting Engineers, 2003; Amiri, 2005; Taheri et al., 2005 and references therein). In two international publications, Karimi and Taheri (2010) and Heidari et al. (2011) presented some GIS-based thematic maps, but did not develop any predictive model or assessed probability of sinkhole occurrence. This work presents for the first time sinkhole magnitude and frequency relationships and sinkhole susceptibility maps of the Kabudar Ahang and Razan–Qahavand plains in northern Hamadan province, western Iran, applying the analytical hierarchy process (AHP) approach. This method was used by Jiang et al. (2005) to produce a country-wide sinkhole susceptibility zonation in China assigning weights to qualitative variables. To our knowledge, this is the first contribution that explores the practicality of the AHP method to assess sinkhole susceptibility in a specific region and incorporating quantitative variables, and one of the very few articles that makes an attempt to generate magnitude and frequency scaling relationships with a comprehensive sinkhole inventory (Galve et al., 2011).

The approaches illustrated in this paper could be satisfactorily applied in the growing number of areas worldwide affected by sinkhole damage. The increase in the sinkhole hazard and risk, similar to the region studied in this work, is frequently related to water table declines caused by aquifer over-exploitation (e.g., Waltham, 2008; Dogan and Yilmaz, 2011; García-Moreno and Mateos, 2011; Aurit et al., 2013) or dewatering for mining (e.g., Sprynskyy et al., 2009; Yang et al., 2015).

2. Study area and geological setting

The study area, covering 6532 km^2 of which 3402 km^2 correspond to alluvial plains, is located in the Zagros Orogenic Belt, and more specifically, in the northern sector of Hamadan province, western Iran (Fig. 1a, b). According to the catchment classification of the Iranian Ministry of Energy, it corresponds to the Kabudar Ahang and Razan–Qahavand subcatchments (KRQ), both within the Hoz-e soltan of Qom watershed (Fig. 1b). The Zagros Orogenic Belt consists of four main NW–SE trending structural zones, from NE to SW; Urumieh–Dokhtar Magmatic Assemblage, Sanandaj–Sirjan, High Zagros Belt, and Zagros Simply Folded Belt (Ghasemi and Talbot, 2006). The KRQ is located in the Sanandaj–Sirjan zone, in which the rocks show the highest degree of deformation of the Zagros orogen (Fig. 1a).

The analyzed area essentially consists of an intramontane depression whose floor is dominated by alluvial environments, locally interrupted by inliers of Mesozoic and Tertiary rocks (Fig. 1c). The exposed geological units range in age from Jurassic to Quaternary, and the Mesozoic rocks are affected by a variable degree of metamorphism. The Jurassic rocks, mostly exposed in the northeastern and southwestern sectors of KRQ, mainly consist of schists, limestone and marls, and are slightly metamorphosed in the latter sector. The Cretaceous system is represented by shales and marly limestone in the northeast, and an orbitolina-bearing limestone sequence on the southern margin of the depression. The Tertiary succession, mainly Oligo-Miocene, includes green volcanic tuffs, marls, marly limestone and limestone (Qom Formation). The soluble units of the Qom Formation constitute the main bedrock underlying the thick detrital sequence in the plains (Fig. 1d). The Quaternary sediments, which locally reach 150 m in thickness, are mainly composed of alluvial facies.

The structure is characterized by a sequence of gentle NW–SE trending anticlines and synclines with a concordant topography; the anticlines typically form ranges, whereas the synclines are buried by alluvium (Fig. 2a). Furthermore, major faults with dominant N10E and N75E trends were recognized in the limestone outcrops of Hamakasi area, where the majority of the sinkholes have been reported (Fig. 2b, c, d).

3. Materials and methods

3.1. Field and laboratory investigation

All the available papers and reports were reviewed to gather data on multiple aspects, especially geology, hydrogeology, geophysics and geotechnics. Particularly useful were the reports supplied by the Hamadan Regional Water Co. The field surveys included (1) systematic recording of sinkhole location and characteristics, (2) description and sampling of surficial deposits and bedrock units, and (3) examination and measurement of fractures and faults. Additional data were obtained in the laboratory by means of granulometry and calcimetry measurements of surficial formations, and the examination of thin sections from rock samples under a petrographic microscope.

A total of 175 joints were measured in the densely fractured Oligo-Miocene limestones of the Qom Formation exposed in the surroundings of Hamakasi village. The strike of the fractures shows two prevalent directions; N10E and N75E (Fig. 2b). The trend of the former set coincides with that of a transverse fault system that seems to play a relevant role in the subsidence phenomenon, as suggested by the orientation of the sinkhole alignments.

Six samples of surficial deposits were collected from exposures associated with the scarped edges of sinkholes Nos. 6, 32, 34, 35, 36 and 43 (Table 1). Granulometric analyses indicate that they have a relatively uniform grain size distribution (well-sorted) and mainly consist of silty-clay and clayey-sand. The deposits from a borehole 115 m deep drilled next to sinkhole No. 8, close to Jahanabad village (Table 1), show a change to clayey silt with interbeds of silty and clayey sand towards the bottom. The plasticity index of the sampled deposits range from 10.3 to 21% in the case of the silts and clays, and around 23% for the clayey sand (Zamiran Consulting Engineers, 2003). Those characteristics suggest that the sediments are non-collapsible, except in those locations where soils rich in silt and/or fine-sand contain intergranular carbonate cements susceptible to dissolution. That is, the soils remain stable until the bounding carbonates dissolve by circulating water and the loosely-packed granular structure collapses (hydrocompaction).

The karstified Qom Formation mainly consists of biomicrite and bioclastic packstone, according to Dunham's (1962) classification.

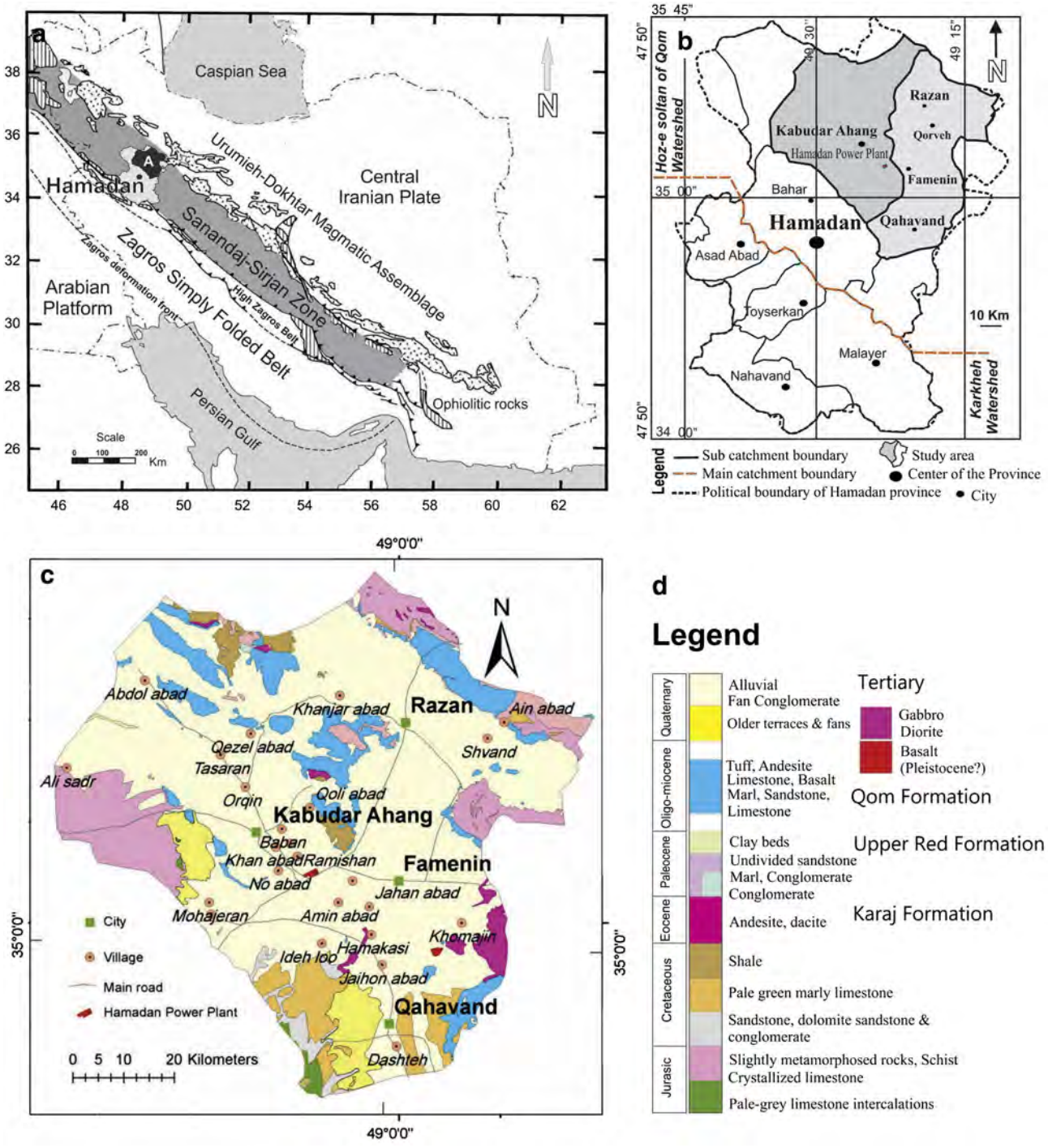

Fig. 1. (a) Location map of the study area in the Zagros Orogenic Belt and Hamadan province in Iran. (b) Distribution of the studied sub-catchments (gray pattern) within the Hoz-e soltan of Qom watershed. (c and d) Geological map and legend (Geological and Mineral Survey of Iran, 1979).

Calcimetry on limestone samples collected from Hamakasi area, Qoli Abad mount and Qare Lar outcrop, provide carbonate contents of 94.8%, 88.4% and 90.5%, respectively, indicating that it is a relatively pure limestone. Visual estimation on thin sections indicates an average primary porosity of around 10%, suitable for karstification. Cave, kamenitzas (solution pits) and solutionally-widened joints are common in limestone outcrops near Hamakasi and Qoli Abad villages. Solution cavities have been encountered by borehole drilling in Jahan Abad within the carbonate bedrock.

3.2. Sinkhole inventory and nomenclature

Since 1989, an increasing number of sinkhole occurrences have been reported in the study area. This ground subsidence phenomenon severely threats human structures like rural settlements and the Hamadan Power Plant (or Shahid Mofatteh Power Plant; Fig. 3). The closest reported sinkhole to this critical facility was located at a distance of 1.5 km (sinkhole No. 11). In 2004, a sinkhole 10 m across formed at a distance of around 100 m from a school (sinkhole No. 36). Some

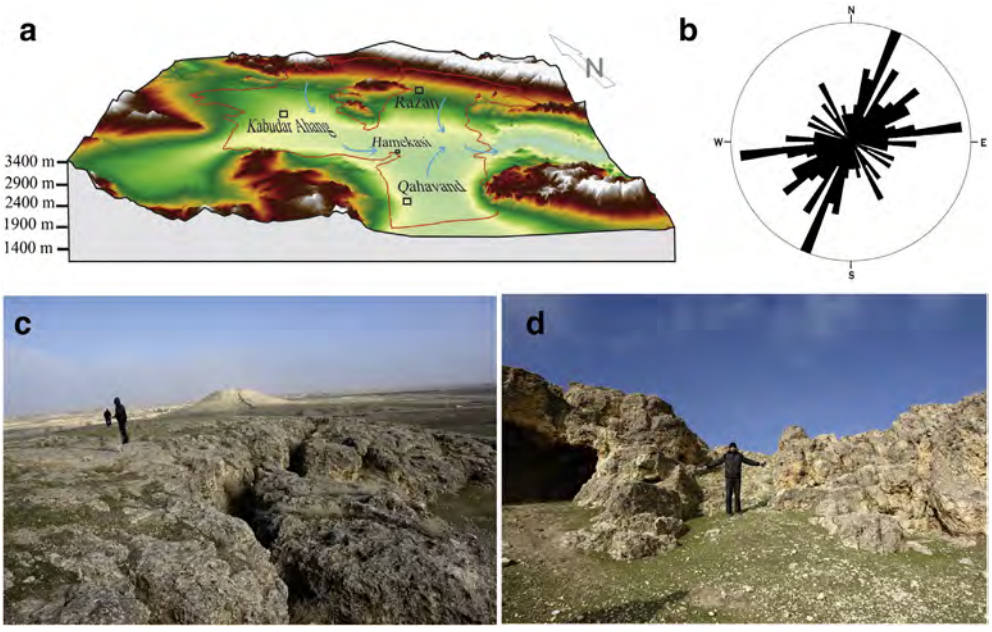

Fig. 2. (a) 3D relief model of the study area. The arrows indicate groundwater flow direction. (b) Rose diagram produced with 175 fractures and joints measured on limestone outcrops around Hamakasi village. (c) Fault in a limestone outcrop in the surroundings of Hamakasi village. Open ground fissure associated with the tilted downthrown block suggests recent tectonic activity. Sinkholes have formed recently associated with this E–W trending fault. (d) Person pointing to the margins of a fault breccia in Hamakasi village area.

subsidence events correspond to the reactivation of pre-existing sinkholes, as revealed by geomorphic evidence and accounts from local people. This indicates that the instability phenomenon has operated in the area for long time, although with a much lower frequency until groundwater abstraction started to have a significant impact on the alluvial-karst aquifer. Table 1 compiles the 49 sinkholes recorded in KRQ, providing information on their location, main morphometric parameters, typology, and chronology. Fig. 3a illustrates the spatial distribution of the inventoried sinkholes. There are some doubts about the three sinkholes labeled with asterisks in Table 1, since they may be related to the collapse of either karst cavities or old qanats (tunnels excavated for water supply and irrigation). In most cases, holes related to the collapse of qanats are clearly distinguishable because of their spatial association with known excavations and their alignments concordant with the qanat orientations. Most of the sinkholes are ascribed to the collapse subsidence mechanism, showing a steep-sided subcircular geometry. The majority are associated with outcrops of the Qom Formation and agricultural farms around Hamakasi village.

The major axial length (D) of the inventoried sinkholes ranges from 100 m to 1.5 m, with an average value of 14.4 m and a standard deviation of 16.7 m. Depth values also cover a wide range, from 30 m to 1.5 m. The mean value and standard deviation for this parameter are 6.2 m and 6.7 m, respectively. Most of the sinkholes are slightly elongated. The elongation ratio of the depressions (major axial length/minor axial length) varies from 1 to 6, and has an average value of 1.4. A significant proportion of the sinkholes reach large volumes, indicating the presence of big cavities and/or a high density of voids in the subsurface; the sinkhole volume should be considered as a minimum estimate of the volume of the subjacent cavities (e.g. Gutiérrez, 2010). If we estimate the volume of the depressions multiplying the depth of the sinkholes by the area of a circle with a diameter given by the measured minor axial length, we obtain a maximum value larger than 20,000 m^3 (sinkhole No. 27). Around 37.8% of the sinkholes have volumes greater than 1000 m^3.

3.3. Factor weighting by AHP and susceptibility assessment

Analytical hierarchy process (AHP) is a structured approach proposed by Saaty (1977, 1980, 2001) for analyzing complex decisions taking into consideration a large number of factors or criteria. The decision-making process is based on the decomposition of the problem into a hierarchy of simpler sub-problems and their systematic and independent evaluation (Tzeng and Huang, 2011; Donevska et al., 2012). In the AHP, decision makers or evaluators, based on their judgments and the available quantitative and qualitative data, assess the relative weight of the decision criteria of the hierarchy for evaluating the alternatives. The different criteria are weighted through a pairwise comparison method. In the subsequent step, numerical priorities are calculated for each of the decision alternatives. The results of the AHP are largely dependent on the knowledge and experience of the experts that select and weight the criteria considered in the decision process (Dweiri and Al-Oqla, 2006; Ho, 2008).

In this work, sinkhole susceptibility has been preliminarily assessed considering the relative weights assigned to eight selected controlling factors (criteria) and to the different classes of each one (subcriteria) (Fig. 4). Initially, the criteria and subcriteria have been weighted performing paired comparisons on square matrixes. To evaluate the relative importance of each factor for sinkhole formation with respect to another one, the Saaty (1980) ranking scale for pairwise comparisons has been applied (Table 2). The scale uses 17 scores, from 1 to 9, plus their reciprocal values (1/9, 1/8, 1/7, 1/6, 1/5, 1/4, 1/3, 1/2, 1, 2, 3, 4, 5, 6, 7, 8, 9). The minimum value 1/9 represents the least relative influence, and score 9 the highest relative significance on sinkhole formation. Scores are given to the cells of the square matrix on one side of the diagonal, and the diagonal entries are always 1; i.e. each factor has an equal value to itself (see Table 3). The scores on the other side of the diagonal, which replicate the pairwise comparisons reversely, correspond to the reciprocal values. Consequently, only the upper triangular portion of the matrix needs to be completed. The relative weight of each criterion is obtained by normalizing the eigenvectors of each element of the matrix (Donevska et al., 2012; Munier, 2011).

An important step of the AHP is to evaluate the consistency of the ratings. This can be carried out calculating the consistency index (CI) and the consistency ratio (CR) (Tzeng and Huang, 2011). The consistency index is defined by equation:

$$CI = \frac{\lambda\,max - n}{n - 1} \quad (1)$$

Table 1
Data from the KRQ sinkhole inventory. D: major axial length (m), d: minor axial length (m), asterisks denote sinkholes of doubtful origin, which may be related to karst voids or anthropogenic cavities, like old qanats or abandoned water wells.

No.	Location	UTM		D (m)	d (m)	Depth (m)	Nomenclature	Date of occurrence
		E	N					
1	Amir abad	289590	3901017	–	–	–	Cover suffusion sinkhole	1999
2	Bizanjerd	313024	3879519	20	16	3	Cover suffusion sinkhole	1998
3	Bizanjerd	312268	3875934	3	2.5	6	Cover suffusion sinkhole	1998
4	Bizanjerd	311513	3877458	3	2.5	3	Cover suffusion sinkhole	Unknown
5	Bizanjerd	312370	3876038	4	3.5	2	Cover suffusion sinkhole	1989
6	Baban	295576	3899807	21	20	20	Cover collapse sinkhole	2008
7	Baban	295495	3899780	5	4	8	Cover collapse sinkhole	2009
8	Jahan abad	315478	3883662	23	20	17	Cover collapse sinkhole	1994
9	Jahan abad	315512	3883472	33	12	1.5	Cover suffusion sinkhole	1995
10	Hesar	279627	3901716	3	2	1	Cover suffusion sinkhole	1998
11	Khan abad	295344	3894429	5	4	3	Cover suffusion sinkhole	1995
12	Kerd abad	299573	3888825	22	17	8	Cover collapse sinkhole	1995
13	Kerd abad	298819	3888249	31	24.5	12	Cover collapse sinkhole	2003
14	Kerd abad	299452	3888739	28	25	20	Cover collapse sinkhole	2004
15	Kerd abad	298882	3888391	38	37.5	8	Cover collapse sinkhole	2008
16	Kerd abad	298888	3888373	43.5	20	5	Cover collapse sinkhole	2009
17	Kerd abad	298888	3888373	–	–	–	Cover collapse sinkhole	2010
18	Kahriz*	311545	3877455	5	4	2	Cover suffusion sinkhole	Unknown
19	Gondejin	290945	3893667	10	8	2	Cover suffusion sinkhole	Unknown
20	Famenin	315290	3887200	20	15	30	Cover collapse sinkhole	2002
21	Sari tapeh*	328147	3876434	2	1.5	5	Cover suffusion sinkhole	2001
22	Sari tapeh*	328155	3876443	1.5	1.5	1.5	Cover suffusion sinkhole	2001
23	No abad	296997	3889035	14	11	16	Cover suffusion sinkhole	1999
24	Negar khatoon	310917	3890981	4	3.5	4	Cover suffusion sinkhole	1997
25	Qare chay river	314227	3881089	20	18	10	Cover collapse sinkhole	Unknown
26	Hame kasi	313857	3877387	2.5	1.5	1.5	Bedrock collapse sinkhole	old
27	Hame kasi	313833	3873060	100	80	4	Cover sagging & suffusion sinkhole	old
28	Hame kasi	313844	3877187	15	5	4	Bedrock collapse sinkhole	old
29	Hame kasi	313809	3877225	6	1	5	Bedrock collapse sinkhole	old
30	Hame kasi	313832	3873060	6	4	3	Bedrock collapse sinkhole	old
31	Hame kasi	313345	3879084	6.6	6	4	Cover suffusion sinkhole	1992
32	Hame kasi	314439	3877234	9	5	10	Cover collapse sinkhole	2010
33	Hame kasi	314121	3877028	9.5	8.5	10	Cover collapse sinkhole	2011
34	Hame kasi	314135	3877028	8.7	8.6	3	Cover collapse sinkhole	2004
35	Hame kasi	314209	3876811	13.5	8.3	6	Cover collapse sinkhole	Unknown
36	Hame kasi	314375	3877350	10	10	20	Cover collapse sinkhole	2004
37	Hame kasi	312841	3875380	5	4	3	Cover suffusion sinkhole	1996
38	Hame kasi	313254	3879076	11.8	10	3	Cover suffusion sinkhole	1992
39	Hame kasi	313211	3879101	23	20	1	Cover suffusion sinkhole	1992
40	Hame kasi	313891	3876783	2.5	1.6	1	Cover suffusion sinkhole	1999
41	Hame kasi	314376	3877351	15	15	1	Cover suffusion sinkhole	1992
42	Hame kasi	314089	3877762	10	8	1	Cover suffusion sinkhole	1992
43	Hame kasi	314365	3877325	34	28.5	3	Cover suffusion sinkhole	1992
44	Hame kasi	312885	3875532	3	2.5	1.5	Cover suffusion sinkhole	1996
45	Hame kasi	312849	3875387	3	2.5	1.5	Cover suffusion sinkhole	1996
46	Hame kasi	313833	3877177	6	5	0.5	Cover sagging sinkhole	Unknown
47	Hame kasi	313827	3877209	4	3	0.5	Cover sagging sinkhole	Unknown
48	Hame kasi	313832	3873060	11	?	15	Bedrock collapse sinkhole	old
49	Hame kasi	313748	3877647	2.5	2	0.5	Cover suffusion sinkhole	Unknown

where λmax is the largest eigenvalue of a preference matrix and n is the number of parameters (Ying et al., 2007; Thanh and De Smedt, 2012). In this study these parameters were calculated as λmax = 8.58 and CI = 0.083. For the calculation of the consistency ratio (CR), the consistency index is compared with a random consistency index RI:

$$CR = \frac{CI}{RI} \quad (2)$$

The RI values have been tabulated by Saaty (1977) as a function of n. Consistency ratios higher than 0.1 suggest untrustworthy judgments, indicating that the comparisons and scores should be revised. In this investigation we have selected eight parameters. Consequently, RI is 1.41 according to Saaty's (1977) table, and CR is 0.059 according to Eq. (2). The obtained consistency ratio is lower than 0.1, suggesting coherence among the pairwise comparisons. In this study, the sinkhole susceptibility indexes have been calculated through a weighted linear combination (WLC) of the considered controlling factors and the classes of each factor (Voogd, 1983). The susceptibility index for each pixel is given by the summation of the products of the weights assigned to each criterion and subcriterion, according to equation:

$$SSI = \sum_{j=1}^{N} Wjwij \quad (3)$$

where SSI is the sinkhole susceptibility index (or final score), Wj the weight of the controlling factor j, wij the weight of class i of factor j, and N is the number of factors considered in the model. The SSI values obtained for 250 m pixels have been divided into four equal classes, in order to represent four susceptibility classes in the final model: very high, high, moderate and low. The natural break classification method, commonly used in landslide susceptibility mapping, was used to categorize the susceptibility classes (Falaschi et al., 2009; Bednarik et al., 2010; Pourghasemi et al., 2012, 2013).

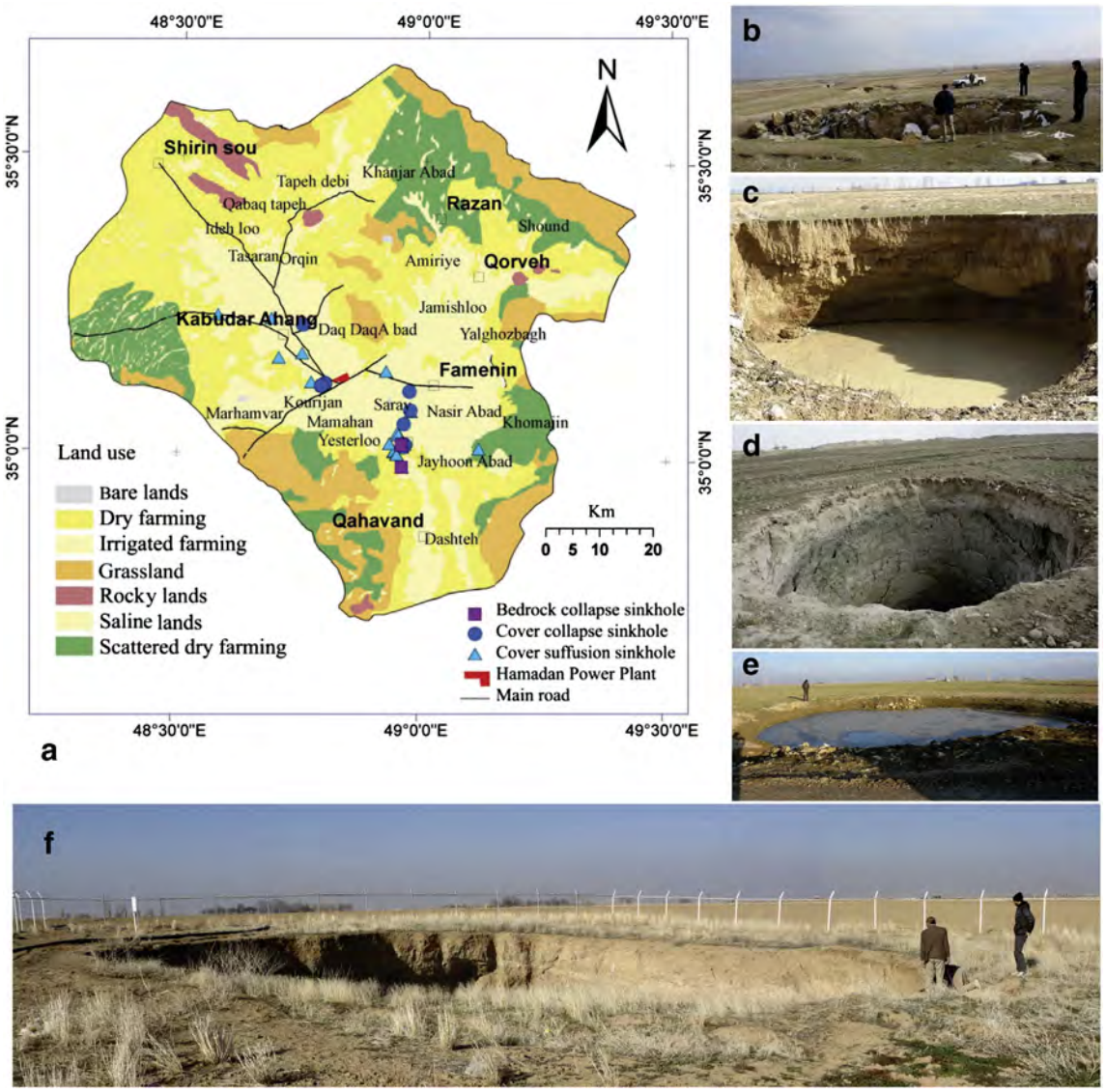

Fig. 3. (a) Location of the KRQ sinkholes on a land-cover map. (b) Bedrock collapse sinkhole 15 m in diameter in Hamakasi area (No 28). (c) Cover collapse sinkhole 31 m across with overhanging walls near Kerd Abad (No 13). Water tables exposed in the bottom of the depression. (d) Cover collapse sinkhole 8.7 m in diameter at Hamakasi area (No 34), Note unloading cracks on its nearly vertical walls. (e) Cover suffusion sinkhole in Jahan Abad area (No 9, 33 m across). Ponded water related to a perched water body above the phreatic zone. (f) Baban cover collapse sinkhole, 21 m across and 20 m deep (No. 6).

In a subsequent step, the prediction capability of the preliminary susceptibility model has been assessed independently calculating the percentage of the inventoried sinkholes in each susceptibility class. New multiple sinkhole susceptibility models have been generated varying the relative weight of the factors and their classes, especially those with higher influence on the final score. The apparently most reliable susceptibility model has been identified through evaluation in a trial and error process.

4. Magnitude and frequency relationships

The probability distribution of the size of the sinkholes can be analyzed considering the major axial length (D) of the 47 sinkholes with morphometric data and the number of sinkholes that equals or exceeds the different values. The major axial length was selected, since this is the most critical morphometric parameter from the risk and engineering perspective (Gutiérrez, 2010; Gutiérrez et al., 2014). A graph plotting major axial length in logarithmic scale, and probability (P), shows a linear trend, which can be described with a high goodness-of-fit ($R^2 = 0.97$) by a logarithmic function (Fig. 5):

$$P = -0.2933 \ln D + 1.1605.$$

It seems that the obtained function adequately models the smallest and largest sinkholes. This is probably because the largest sinkhole of the inventory may correspond to the coalescence of several depressions. Moreover, the number of small sinkholes may be skewed (underestimated) due to the difficulties related to their detection. Small depressions are more difficult to identify and tend to be rapidly filled by local people (e.g. Gutiérrez et al., 2007). A regression after removing the upper and lower bounds of the axial length data set (100 m, and 1.5 m) provides a function with a higher goodness-of-fit ($R^2 = 0.99$):

$$P = -0.336 \ln D + 1.2567.$$

According to this scaling relationship, the relative probability of sinkholes reaching axial lengths of 5 m, 10 m, 20 m, and 30 m, are

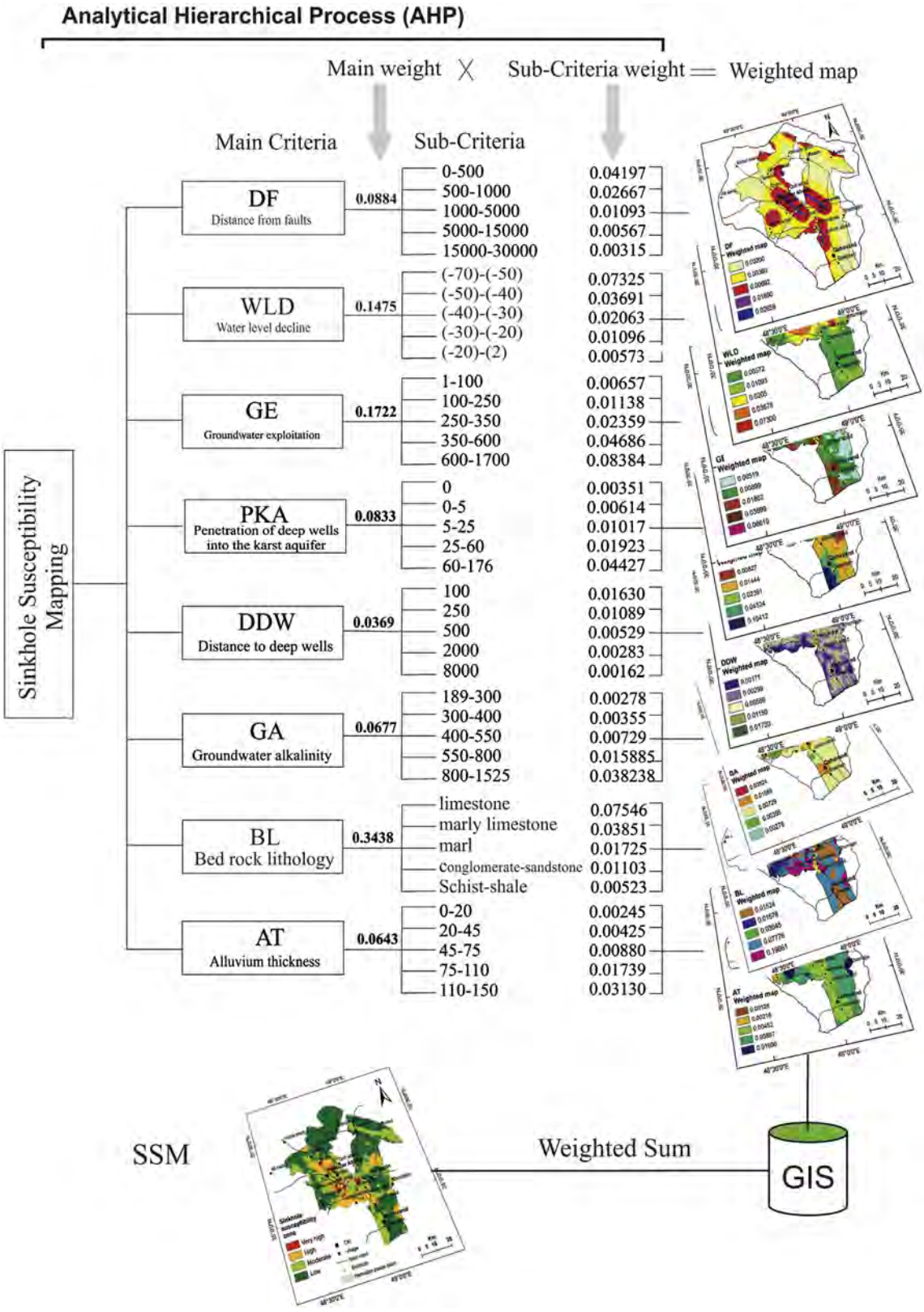

Fig. 4. Flow diagram showing the hierarchy of the AHP for weighting the controlling factors, as the basis for constructing the sinkhole susceptibility map. The latter is produced by calculating the sinkhole susceptibility index as a weighted sum and classifying the index values into four equal intervals corresponding to four susceptibility classes.

approximately 0.71, 0.48, 0.25, and 0.11, respectively. This means that, for instance, the probability for a new sinkhole having a major axial length equal or higher than 20 m is around 25%.

A total of 41 sinkholes, out of the 49 inventoried ones, have formed between 1989 and 2011. The date of 33 of them is known, whereas the age of the 8 remaining ones can only bracketed at 1989–2011.

Table 2
Saaty (1980) scale for pairwise comparisons.

Preference judgments	Ranking
Both criteria are equally important or preferred	1
One criterion is moderately more important than the others (weak preference)	3
One criterion is strongly more important than the others	5
One criterion is very strongly more important than the others	7
One criterion is extremely more important than the others	9
Intermediate values	2–4–6–8

This data indicate an average annual sinkhole frequency of 1.8 sinkholes/yr for that time period. This must be considered as a minimum temporal frequency estimate, since most probably our sinkhole inventory is incomplete. In order to assess the minimum probability of occurrence of sinkholes with different diameters, the magnitude and frequency relationship of the 41 inventoried sinkholes formed in the period 1989–2011 has been explored considering the major axial length of the depressions. The annual frequency of sinkholes (Na) with major axial lengths greater than or equal to D and the D values, have been plotted representing the size in logarithmic scale (Fig. 6). The graph also shows a clear linear trend and a very good fit ($R^2 = 0.99$) with a logarithmic function:

$$Na = -0.56 \ln D + 2.1439.$$

According to this optimistic scaling relationship, and assuming that the subsidence phenomenon in the future will have similar magnitude and frequency patterns, we can expect that sinkholes with diameters larger than or equal to 5 m, 10 m, 20 m, and 30 m, will have maximum recurrence intervals of 0.8, 1.17, 2.14, and 4.18 years, respectively.

5. Sinkhole susceptibility mapping

5.1. Controlling factors

A number of natural and anthropogenic factors are involved in the development of sinkholes in the KRQ area (Taheri, 2005). The factors can be grouped into three main groups: engineering–structural geology, hydrogeology, and stratigraphy (Table 2). The main factors of the first group include fault distribution and geotechnical properties of rocks and cover deposits, which determine their rheology (subsidence mechanisms). Regarding hydrogeology, groundwater flow paths, the secondary permeability within the karst aquifer, including cavities, and the water-table decline caused by aquifer overexploitation, are considered to play a significant role in sinkhole development. The characteristics and thickness of the overburden underlain by karstified limestone also have a significant influence on the probability of sinkhole occurrence. Other factors including irrigation type, land use, groundwater aggressiveness, geotechnical conditions, and Quaternary pneumatolytic volcanism, should have some influence on sinkhole genesis, but their contribution is difficult to assess through statistical approaches due to the shortage of data.

Table 3
Pairwise comparison matrix constructed for calculating the main weight for the criteria (factors) used to assess sinkhole susceptibility.

	DF	WLD	GE	PKA	DDW	GA	BL	AT	Weights
DF	1	0.5	0.5	1	5	2	0.2	1	0.08841
WLD	2	1	1	2	5	3	0.33	2	0.14751
GE	2	1	1	3	5	3	0.5	3	0.17228
PKA	1	0.5	0.33	1	5	0.5	0.2	2	0.08334
DDW	0.2	0.2	0.2	0.2	1	0.33	0.17	0.5	0.03695
GA	0.5	0.33	0.33	2	3	1	0.13	1	0.06775
BL	5	3	2	5	6	8	1	4	0.34386
AT	1	0.5	0.33	0.5	2	1	0.25	1	0.06431

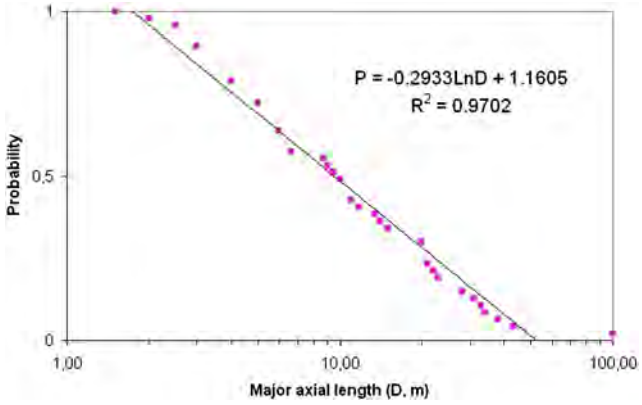

Fig. 5. Plot showing the magnitude and probability relationship obtained with the 47 inventoried sinkholes with available morphometric data. A better fit is obtained when removing the lower and upper bounds of the data set. See explanation in text.

Based on the information and findings presented in previous studies (Zamiran Consulting Engineers, 2003; Amiri, 2005; Taheri, 2005; Taheri et al., 2005; Ouhadi and Bakhshalipour, 2010; Ouhadi and Goodarzi, 2010; Khanlari et al., 2012), as well as new data gathered for this work, eight parameters were selected out of the available spatial data layers in order to assess sinkhole susceptibility (Table 4, Figs. 4, 7 and 8): distance to faults (DF), water level decline (WLD), groundwater exploitation (GE, rate of pumping in public water wells in million cubic meters per year), penetration of deep wells into the karst aquifer (PKA), distance to deep wells (DDW), groundwater alkalinity (GA), bedrock lithology (BL) and alluvium thickness (AT).

5.1.1. Distance to faults (DF)

Faults, both exposed and concealed, may influence the spatial distribution of sinkholes. Fault zones in carbonate rocks are commonly characterized by higher hydraulic conductivity and more cavernous conditions. Secondary porosity may be particularly high where faults juxtapose soluble formations against insoluble and impervious rocks (contact karst). Moreover, faults may act as preferential pathways for ascending deep-sourced fluids that may enhance groundwater aggressiveness by the incorporation of gasses like CO_2 or H_2S. In outcrops of the Qom Formation in Hamakasi village area, some sinkholes occur associated with faults or areas with a higher joint density. Moreover, effervescence in the water extracted from some wells suggests input of dissolved gases from deep sources. Further investigations, including isotopic analyses, are necessary to constrain the composition and origin of those gases. The DF map has been produced by a buffering method considering five classes (Fig. 7a). The weighted map incorporated the main weight of the variable (0.08) and the relative weights of the classes (Fig. 8a).

5.1.2. Water level decline (WLD)

A number of hydrogeological factors may play a significant role in sinkhole development, including aquifer permeability, transmissivity and diffusivity, hydraulic gradient, flow direction, rate and regime (laminar vs. turbulent). However, it is not possible to produce reliable spatial data layers of these factors due to the limited and sparse available data. Water level decline (WLD) related to aquifer over-exploitation or mining-related dewatering is one of the most common sinkhole-inducing anthropogenic factors (e.g. Newton, 1984; Gao, et al., 2001; Waltham et al., 2005). The main detrimental effects of the water-table decline include (Gutiérrez, 2010): (1) loss of buoyant support on sediments, with the consequent increase in the effective weight of cavity roofs; (2) local increase in groundwater velocity, especially in depression cones; and (3) replacement of phreatic flows by downward vadose

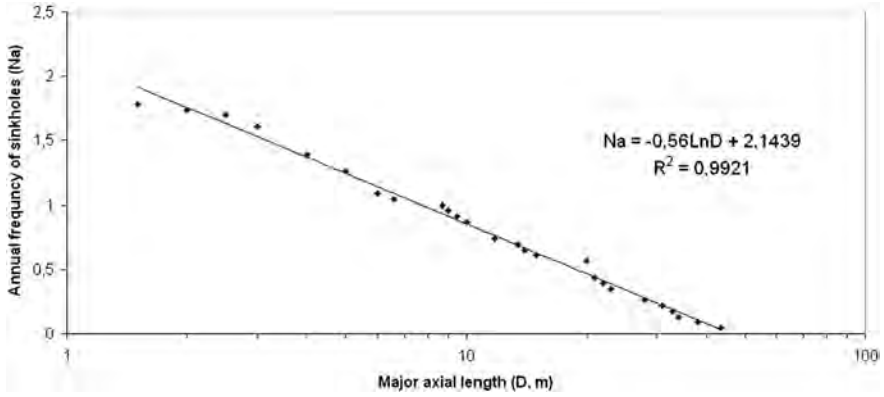

Fig. 6. Plot showing the magnitude and frequency scaling relationship obtained with the 41 inventoried sinkholes formed over a period of 23 years (1989–2011). Na is the annual frequency of sinkholes with a major axial length larger than or equal to D. The hazard values derived from this regression must be considered as minimum estimates (optimistic), since the analyzed inventory is most probably incomplete.

flows with a greater capability to cause internal erosion. This effect is particularly significant when the water table declines below the rockhead.

A WLD map of the study area has been prepared computing the water-table decline over a period of 22 years (1988–2010), using data from 65 piezometers and applying the IDW (inverse distance weighted) method (Fig. 9c). The water-table decline since 1988 has reached 75 m in the central sector of the study area. Although some sinkholes have occurred in zones affected by significant drawdowns, like the Hamadan Power Plant area, others do not show a clear spatial correlation (Fig. 8b). The WLD values have been divided into 5 classes (Fig. 7b). Subsequently, a WLD weighted map has been produced multiplying the main weight of the factor (0.14751) by the weights assigned to each class (Fig. 8b).

5.1.3. Groundwater exploitation (GE)

Most probably, the amount and rate of groundwater abstraction has a significant influence on sinkhole development. Together with other factors like transmissivity and recharge rate, abstraction determines the groundwater level decline. Moreover, water pumping from alluvial aquifers with a high proportion of fine-grained facies may (1) increase the potential for hydrocompaction, and (2) cause the suction of sediments with the consequent generation of voids and the weakening of the soil cover. Seepage forces, effective stresses and flow turbulence are conditioned by the volume and rate of groundwater exploitation. Groundwater pumping has greatly increased in the northern sector of Hamadan province over the last two decades due to rapid agricultural, industrial and urban development. An annual groundwater exploitation map has been constructed integrating data from dossiers of 3850 public water wells of Hamadan Regional Water Co. updated in 2012, and applying the IDW method. Locally, the annual volume of groundwater exploitation by deep and shallow water wells exceeds 800 MCM/yr (million m^3/year). There seems to be a reasonable spatial correlation between the areas with higher water demand and the distribution of sinkholes. In the GE map, the variable has been classified into five categories: 1–100, 100–250, 250–350, 350–600, and 600–1700 MCM/yr (Fig. 7c). The GE weighted map has been produced multiplying the weight of the variable (0.17) by the relative weight estimated for each class (Fig. 8c).

5.1.4. Penetration of deep wells into the karst aquifer (PKA)

The depth of the wells that extract water from the alluvial aquifer varies from 60 to 150 m. In the vicinity of Hamadan Power Plant, there are also 230–260-m deep wells that penetrate more than 140 m into the bedrock. Additionally, the onset of the occurrence of collapse sinkholes coincides with the drilling of deep wells into the karst bedrock. Rod falls during drilling of deep wells penetrating into the limestone bedrock reveals the presence of deeply buried cavities (Karimi and Taheri, 2010). The vertical distance that deep wells penetrate into bedrock may reflect the relative contribution of pumping-induced suction to internal erosion in the karst voids and overburden. The washing out of the sediment filling pre-existing conduits may initiate the downward migration of overburden deposits by suffusion and collapse, as well as the upward propagation of conduits towards the surface. This stopping process is catalyzed by the decline of the water table and the consequent decrease in buoyant support.

The spatial and temporal correlation clearly indicates that water abstraction from the karst aquifer plays an instrumental role in the formation of human-induced sinkholes, and it seems reasonable to propose that the higher the penetration of wells into the karst bedrock, the higher the impact. The PKA variable has been discretized into five classes (Fig. 7d). The PKA weighted map has been constructed multiply in the main weight of the variable (0.083) by the weights of the classes (Fig. 8d). Higher weights are given to the wells that penetrate deeper into the bedrock and the lower ones to wells confined to the alluvium.

5.1.5. Distance to deep wells (DDW)

Most of the recorded sinkholes are located in the vicinity of deep production wells. Local people witnessed turbidity changes in deep wells spatially and temporally associated with cover collapse sinkhole occurrences. For instance, soon after the formation of the Jahan Abad cover collapse sinkhole (No. 9), one of the neighboring wells became turbid during 24 h (Khanlari et al., 2012). Sand pumping into production wells has received especial attention in recent years. The enlargement of the screen openings due to poor quality metals (unprotected non-galvanized steel), use of unsuitable well screens, and improper design of the gravel pack in tube wells seem to be the main causes of sand pumping in most of the deep wells in the study area. The turbulent flow associated with over-pumping causes the washing out of fine-grained sediment. Unfortunately, we had no direct access to the out washed sediments. As there is no possibility to measure the volume or rate of pumped sediment from the karst conduit network (i.e., human-induced internal erosion from karst conduits), the proximity to deep wells could be considered as a proxy for this factor. The DDW map has been produced by a buffering method and classifying the variable into five classes (Fig. 7e). The weighted map incorporates the main weight of the variable (0.036) and the relative weights of the classes (Fig. 8e).

5.1.6. Groundwater alkalinity (GA)

In natural waters the alkalinity is mainly related to the concentration of bicarbonate ion and, to a minor extent, to the carbonate anion (CO_3^{2-}). Carbonate alkalinity is defined as $HCO_3^- + 2CO_3^{2-}$ (Langmuir, 1997). In most natural waters carbonate alkalinity roughly equals

Table 4
Available raster data layers of potential conditioning factors. The factors used for susceptibility mapping are indicated in bold (HWRC: Hamadan Water Regional Authority).

	Variable	Layer	Source	Description	Evaluation/comments
Geomorphology–structural geology	Sinkhole location	SL	Field survey	Location of recorded sinkholes	Comparison between sinkhole distribution and selected factors
	Distance to faults	**DF**	Geological Survey of Iran	Fault buffers (m)	Zones with higher permeability, lower mechanical strength and contacts between different lithologies (contact karst)
Hydrogeology	**Water level decline**	**WLD**	Calculated from HWRC piezometric data	Elevation difference in the groundwater level between 1986 and 2012.	Loss of buoyant support in sediments overlying cavities within the vadose zone
	Groundwater exploitation	**GE**	HWRC groundwater data base	Groundwater consumption extracted from dossiers on the over 3000 public production wells (million m^3/year)	Identification of the areas with greatest exploitation and human-induced groundwater flow (depression cones)
	Penetration of deep wells into karst aquifer	**PKA**	Extracted from HWRC dossiers of the over 3000 public production wells	Difference between well depth and overburden (alluvial cover) thickness	Location of wells respect to contact of alluvium–karst interface, rate of karst aquifer/or filled cavity depletion
	Distance to deep wells	**DDW**	HWRC wells data base	Production wells buffers	Impact of pumping on local groundwater flow. Potential suction of sand through well screen.
	Groundwater alkalinity	**GA**	Gathered Data available and obtained by authors	Isolines of HCO_3 concentration	Detection of karstification zones
Stratigraphy	**Bedrock lithology**	**BL**	Data from around 330 exploration and production wells processed by the authors	Karst and non-karst bedrock distribution	Suitability for karst development
	Alluvium thickness	**AT**	DEM and isopach map	Alluvium thickness and distribution of rockhead (cover–bedrock contact)	Reflects alluvial thickness and aquifer type abstraction.
Basic maps	Geological units	GEOL.	Geological Survey of Iran	Distribution of lithologies, facies changes, and or the main structural trends	Construction of isopach map in combination with data from exploration wells
	DEM	DEM	DEM	Elevation data	Used to construct of structure contour map of the overburden–bedrock interface
	Hydrography	HYD	HWRC	Distribution of drainage network	Distance of sinkholes to channels
	Geomorphology	GEOM	DEM-field survey	Geomorphological units	Relationship between distribution of sinkholes and other landforms
	Geophysical data	GEOP	Geophysical database of HWRC and other reports	Bedrock units and fault distribution	Detection of subsurface geological features (e.g. faults)
	Main roads	MR	HWRC data base	Local access	Comparing the distribution of sinkholes and infrastructures
	Villages and cities	SET	HWRC data base	Local settlement	Assessing potential relationship between sinkhole and population (human activity) distribution
	Land use map	LU	Soffianian et al. (2011)	Land use spatial distribution	Comparing sinkhole distribution and human activities
Hydrogeological related maps	Pumping wells drilling time	WD	HWRC data base	Groundwater over-exploitation	Assessment of recent human impact on groundwater
	Water wells depth	WWD	HWRC data base	Wells drilled in overburden or overburden and bedrock	Use to estimate amount of penetration into bedrock
	Groundwater level equipotential lines	GLE	HWRC piezometric data	Groundwater flow, current groundwater level	Comparison with piezometeric data and identification of depression cones
	EC	EC	Data available and collected by authors	Groundwater residence time and water quality/aggressiveness	Areas with potentially active karstification
	Calcite saturation indices	CSI	Data available and collected by authors	Karstification capability of groundwater	Areas with potentially active karstification
	CO_2 saturation index	COSI	Data available and collected by authors	Karstification capability of groundwater	Areas with potentially active karstification
	Groundwater temperature	GT	HWRC data base	Karstification capability of groundwater	Areas with potentially active karstification. Location of thermal flows
	Alluvium — overburden isopach map	AO	Data available and collected by authors	Thickness of alluvial deposits and depth to bedrock derived from exploration wells data	Penetration of deep wells into the karst aquifer

total alkalinity (Drever, 1997). High concentration of HCO_3^- in groundwater may indicate extensive dissolution of carbonate rocks and consequently karst development in the bedrock. High HCO_3^- may also indicate nearly saturated water and low dissolution capacity. The HCO_3^- increases along the flow path and may come from far field sources. The HCO_3^- value in the typical karst terrain is around 200 mg/l (e.g. Salvati and Sasowsky, 2002), whereas bicarbonate concentration in some parts of the KRQ exceeds 1500 mg/l. The dissolved bicarbonate may be originated from dissolution of carbonate bedrock by water acidified through the incorporation of rising gaseous CO_2. Alkalinity values

Fig. 7. Thematic maps of the eight factors selected for the production of the susceptibility model: (a) distance to faults (DF); (b) water level decline (WLD); (c) groundwater exploitation (GE); (d) penetration of deep wells into the karst aquifer (PKA); (e) distance to deep wells (DDW); (f) groundwater alkalinity (GA); (g) bedrock lithology (BL); and (h) alluvium thickness (AT).

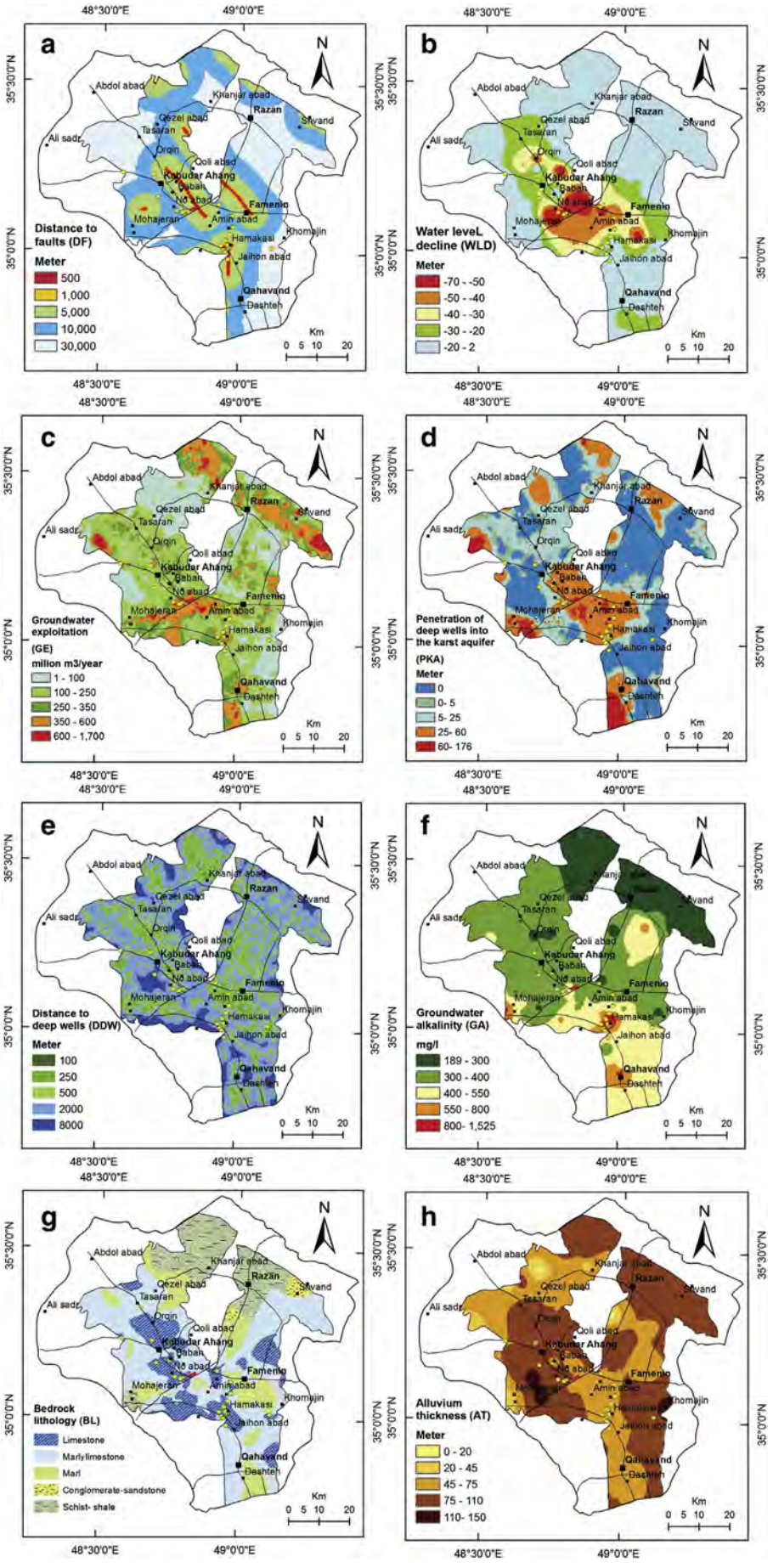
a
Distance to faults (DF)
Meter
500
1,000
5,000
10,000
30,000
b
Water level decline (WLD)
Meter
-70 - -50
-50 - -40
-40 - -30
-30 - -20
-20 - 2
c
Groundwater exploitation (GE)
milion m3/year
1 - 100
100 - 250
250 - 350
350 - 600
600 - 1,700
d
Penetration of deep wells into the karst aquifer (PKA)
Meter
0
0- 5
5- 25
25- 60
60- 176
e
Distance to deep wells (DDW)
Meter
100
250
500
2000
8000
f
Groundwater alkalinity (GA)
mg/l
189 - 300
300 - 400
400 - 550
550 - 800
800- 1,525
g
Bedrock lithology (BL)
Limestone
Marly limestone
Marl
Conglomerate-sandstone
Schist- shale
h
Alluvium thickness (AT)
Meter
0 - 20
20 - 45
45 - 75
75 - 110
110- 150
Abdol abad
Khanjar abad
Razan
Qezel abad
Sivand
Tasaran
Ali sadr
Orqin
Qoli abad
Kabudar Ahang
Babak
Nō abad
Famenin
Mohajeran
Amin abad
Hamakasi
Khomjin
Jaihon abad
Qahavand
Dashteh
Km
0 5 10 20
48°30'0"E
49°0'0"E
35°30'0"N
35°0'0"N
N

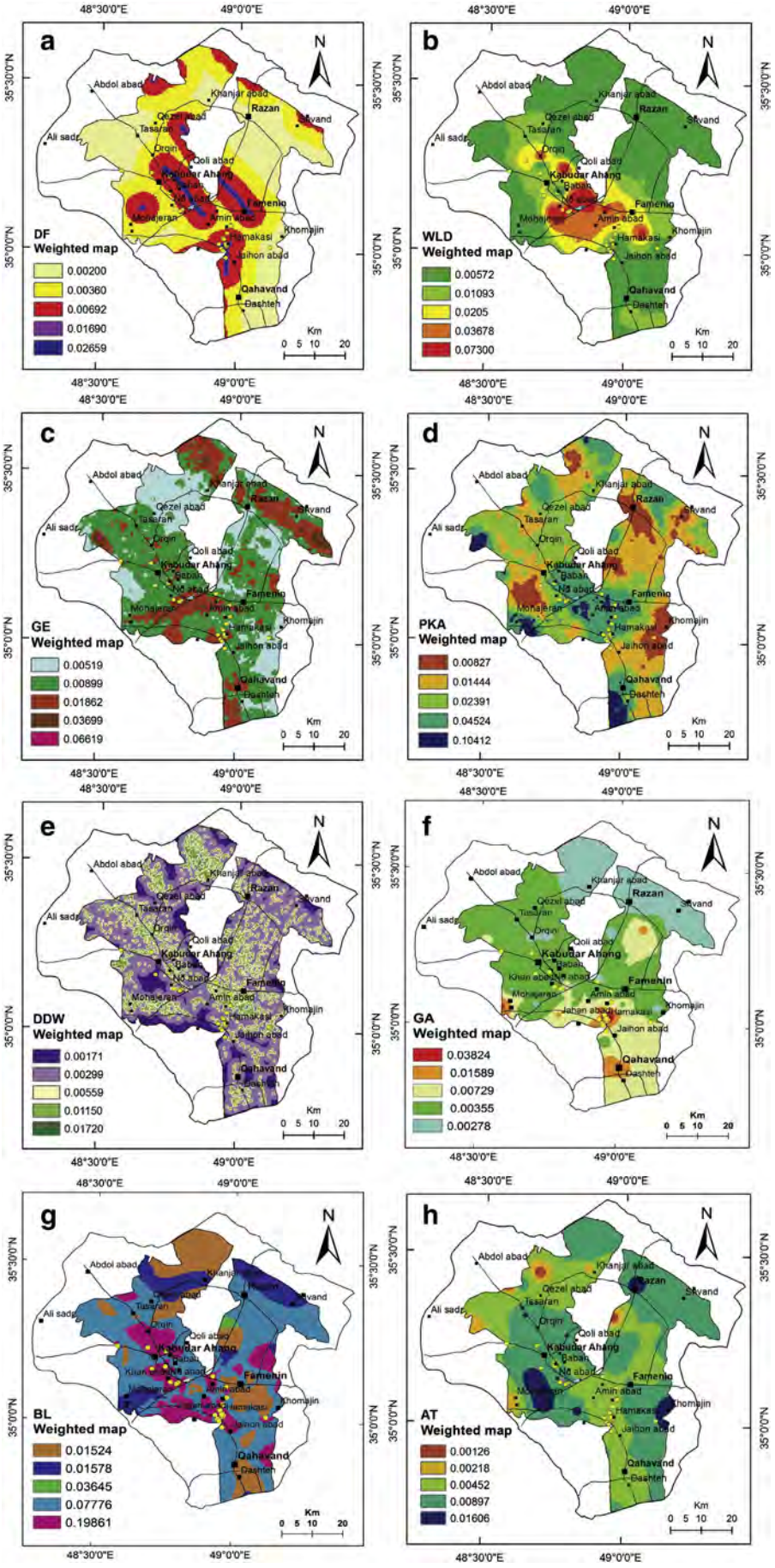
a
DF
Weighted map
0.00200
0.00360
0.00692
0.01690
0.02659
b
WLD
Weighted map
0.00572
0.01093
0.0205
0.03678
0.07300
c
GE
Weighted map
0.00519
0.00899
0.01862
0.03699
0.06619
d
PKA
Weighted map
0.00827
0.01444
0.02391
0.04524
0.10412
e
DDW
Weighted map
0.00171
0.00299
0.00559
0.01150
0.01720
f
GA
Weighted map
0.03824
0.01589
0.00729
0.00355
0.00278
g
BL
Weighted map
0.01524
0.01578
0.03645
0.07776
0.19861
h
AT
Weighted map
0.00126
0.00218
0.00452
0.00897
0.01606
48°30'0"E
49°0'0"E
35°30'0"N
35°0'0"N
N
Km
0 5 10 20
Abdol abad
Khanjar abad
Razan
Sfvand
Qezel abad
Tasaran
Ali sadr
Orqin
Qoli abad
Kabudar Ahang
Babali
Ni abad
Famenin
Mohajeran
Amin abad
Hamakasi
Khomajin
Jaihon abad
Qahavand
Dashteh

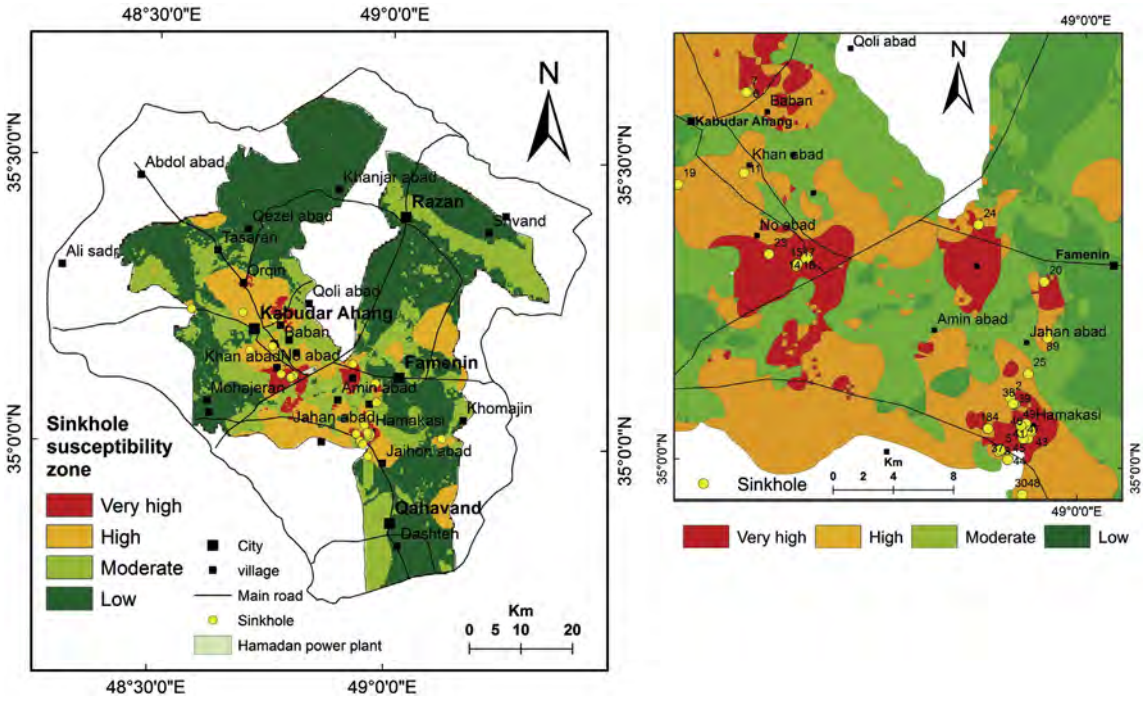

Fig. 9. Sinkhole susceptibility map of the study area and the current location of the sinkholes.

have been obtained from 77 water samples analyses. The GA map depicts five alkalinity classes, from low alkalinity (189–300) to high alkalinity (800–1525) (Fig. 7f). The GA weighted map incorporates the weights of the variable (0.067) and those of the different alkalinity classes (Fig. 8f).

5.1.7. Bedrock lithology (BL)

The presence of karst bedrock is an essential requisite for the development of dissolution-induced sinkholes (Taheri, 2005; Heidari et al., 2011; Khanlari et al., 2012). In the plains, were the bedrock is concealed by Quaternary alluvium, the distribution of lithologies was mainly inferred through projections and interpolations from the geological maps, logs from well logs and geophysical surveys. The bedrock lithology was classified into five categories depending on the inherent karstification potential: limestone, marly limestone, marls, conglomerate-sandstone, and shale-schist (Fig. 7g). According to the AHP calculations for these subcriteria, limestone and shale-schist have the highest and lowest relative weights, respectively. A bedrock weighted-map has been derived from the bedrock lithology map multiplying the main weight of the factor (0.34) by the weights assigned to each lithological class (Fig. 8g). In the preliminary susceptibility model, quite similar relative weights were estimated for the lithologies and marly limestone. The basis of this judgment is that the presence of inter-stratified marls may favor dissolution at the contact between the soluble and impervious units (contact karst). However, the evaluation of multiple models generated with different relative weights for the lithological classes has revealed that susceptibility is significantly higher in the areas with limestone bedrock than in those underlain by marly limestone.

5.1.8. Alluvium thickness (AT)

An isopach map showing the thickness of the alluvial deposits has been constructed using data from 25 exploratory wells. Geophysical data and logs from pumping wells and boreholes have been used to test the validity of the map and refine it. Alluvium thickness is an important factor for sinkhole development. It indicates the thickness of alluvium through which cavities rooted in the limestone bedrock have to propagate upwards to reach the surface and create a sinkhole. Generally, the spatial–temporal frequency of sinkholes decreases with overburden thickness, whereas in the study area the majority of the sinkholes have formed in areas where the Qom Limestone is covered by thick Quaternary alluvium, rather than in sectors with a thin alluvial mantle or exposed bedrock. It seems that the variable alluvium thickness indirectly includes other favorable factors such as higher groundwater exploitation, higher water-table drawdown, and possibly the presence of tectonic structures and mechanically weaker rocks and cover deposits. It appears that alluvium thickness explains sinkhole distribution indirectly because it shows a similar distribution pattern to other above-mentioned hidden factors. An AT map has been produced dividing the variable into five classes: 0–20, 20–45, 45–75, 75–110 and 110–150 (low to high) (Fig. 7h). The AT-weighted map has been constructed multiplying the main weight of the factor (0.064) by the relative weights assigned to each thickness class (Fig. 8h).

6. Discussion and conclusions

Sinkhole hazard has increased dramatically since the 1980s in the northern plains of Hamadan province, western Iran. The spatial and temporal correlation between sinkhole occurrences and groundwater pumping reveals that most of the subsidence events in the study area are induced by aquifer over-exploitation. Groundwater abstraction from the alluvial cover (up to 150 m thick) and the underlying cavernous limestone aquifer has resulted in a decline of up to 75 m in the groundwater level since 1988, locally at a rate higher than 3 m/yr. The physical effects of the water-table decline that favor sinkhole formation

Fig. 8. Weighted maps of the eight factors produced multiplying the main weight of the variable by the relative weights of each class, both estimated by the AHP approach. (a) Distance to faults (DF); (b) water level decline (WLD); (c) groundwater exploitation (GE); (d) penetration of deep wells into the karst aquifer (PKA); (e) distance to deep wells (DDW); (f) groundwater alkalinity (GA); (g) bedrock lithology (BL); and (h) alluvium thickness (AT).

include: (1) loss of buoyant support; (2) increase in groundwater flow velocity associated with depression cones; (3) replacement of slow phreatic flows by gravity-driven downward vadose flows with higher capability to cause internal erosion; and (4) potential suction of fine-grained sediments form sediment-filled cavities in the bedrock and from the alluvial cover.

The sinkhole-related subsidence poses a significant threat for people and human structures, including sensitive facilities like the Hamadan Power Plant. Here, wells up to 260 m deep and penetrating as much as 140 m into the karst bedrock extract groundwater at high rates. Sinkholes have already formed in the vicinity of the power plant, and in 2004 a large cover collapse sinkhole occurred at a distance of 100 m from a school. The sinkholes in the study area have a large damaging potential (severity) and might even cause the loss of human lives due to two main factors: (1) a great proportion of the subsidence events correspond to collapse sinkholes that form catastrophically; and (2) they frequently exceed 20 m in diameter.

The constructed sinkhole inventory, including 49 sinkholes, most of them with chronological and morphometric data, has allowed the calculation of valuable sinkhole hazard estimates. Such hazard values should be considered as minimum (optimistic) values due to two main reasons: (1) the sinkhole inventory is most probably incomplete; and (2) it is likely that the hazard will increase in the near future, as long as the main driving factor (groundwater abstraction) remains. A minimum probability of 1.8 sinkholes/yr has been estimated for the study area, covering 6532 km^2. The magnitude and frequency relationship constructed using the 41 sinkholes with chronological and morphometric data indicates maximum recurrence intervals of 1.17, 2.14 and 4.18 years for sinkholes with major axial lengths equal to or higher than 10, 20 and 30 m, respectively. It is highly desirable to continuously update the sinkhole inventory in the following years, in order to investigate several practical issues: (1) potential changes in the spatial distribution patterns of the subsidence phenomenon (e.g. clustering, alignments, relationship with groundwater abstraction points); (2) temporal evolution of the overall sinkhole temporal frequency; i.e., does the rate at which sinkholes form in the area decrease or increase? and (3) potential variations in the magnitude and frequency relationships.

A preliminary sinkhole susceptibility model was produced in a GIS environment applying the analytical hierarchy process (AHP) approach and considering a selection of eight factors, each categorized into five classes: distance to faults (DF), water level decline (WLD), groundwater exploitation (GE), penetration of deep wells into karst bedrock (PKA), distance to deep wells (DDW), groundwater alkalinity (GA), bedrock lithology (BL) and alluvium thickness (AT). Relative weights were preliminarily assigned to each factor and to their different classes through systematic pairwise comparisons based on expert judgment. A sinkhole susceptibility index was obtained for each pixel from the summation of the products given by the weights assigned to each factor and the corresponding class. The resulting susceptibility index values were then classified into four susceptibility classes (low, moderate, high and very high) for the production of a preliminary susceptibility model.

The inventoried sinkholes, covering a time span larger than two decades of groundwater over-exploitation, have not been used for the development of the susceptibility model. The initial weighting of the factors by expert judgment (systematic pairwise comparisons) was based on theoretical background on karst and sinkhole development, without considering the spatial relationships between the variables and the inventoried sinkholes. Consequently, they can be considered as an independent and representative sample of subsidence events, which can be used to assess the prediction capability of the model (e.g. Galve et al., 2009c). The higher the spatial correlation between the distribution of sinkholes formed in the past and that of the highest susceptibility classes, the higher the prediction rate of the model.

The preliminary sinkhole susceptibility model was evaluated using the sinkhole data layer. Subsequently, multiple models were developed changing the relative weights. Evaluation of those models has allowed us to progressively improve the prediction capability of the models through a trial and error processes. In the susceptibility model with apparently higher prediction capability presented in this work, 51% and 49% of the 49 recorded sinkholes are located within the very high and high susceptibility zones, respectively (Fig. 9). The spatial correlation rises to 55% and 45%, if the 3 depressions with doubtful origin and the 6 old sinkholes with unknown date, probably formed before the anthropogenic lowering of the groundwater level, are disregarded (Table 1). These figures suggest that most of the future sinkholes can be expected to occur within the very high and high susceptibility zones of the map. However, this apparently high prediction rate has a limited usefulness from the risk management perspective, since those two susceptibility classes cover 884.5 km^2 (26% of the total area). It would not be feasible and/or practical to apply mitigation measures in such large area. Therefore, it would be desirable to produce more practical models predicting the distribution of a large proportion of the new sinkholes with more spatially restricted high susceptibility zones.

Bedrock lithology is the factor that received the higher weight (0.343). Obviously, the probability of sinkhole occurrence largely depends on the lithology of the bedrock situated immediately beneath the alluvial cover. There is a group of factors related to groundwater exploitation that have received significantly lower weights (WLD: 0.147; PKA: 0.083; GE: 0.172; DDW: 0.036). However, they implicitly assign the highest weight to the human disturbance that is thought to be the main inducing-triggering factor, with an aggregate value of 0.440. Relatively low values have been ascribed to the remaining factors: distance to faults (0.088), alluvium thickness (0.0643), and groundwater alkalinity (0.068).

The limitations of the model are partly related to the difficulty of gathering data on some relevant geological factors, due to their hidden nature. For instance, the distribution of limestone bedrock, largely concealed by thick Quaternary alluvium, is highly uncertain; the bedrock lithology data layer may have significant inaccuracies. A close examination of the spatial distribution of the inventoried sinkholes reveals that they tend to form clusters and alignments (Fig. 9). A significant proportion of sinkholes occur on an N–S trending belt south of Famenin city, consistently with one of the faults considered in the distance to fault data layer (Fig. 3a). Around 3 km SW of the Hamadan Power Plant, there is a clear sinkhole alignment with a NE–SW orientation, strongly suggesting that subsidence phenomena is controlled by a buried fault or fault system with that trend. However, the distance to fault data layer does not include such inferred fault or any other tectonic structure with a similar orientation.

The model presented in this work has been constructed by weighting a selection of controlling factors. Additional susceptibility models could be generated and evaluated applying other approaches. One alternative is to assess susceptibility on the basis of the statistical relationships between the spatial distribution of inventoried sinkholes and that of different sets of controlling factors. Another alternative is to produce susceptibility models using the spatial distribution of the recorded sinkholes. Susceptibility may be assessed considering parameters like sinkhole density, distance to the nearest sinkhole, or preferred sinkhole orientations. These approaches might allow the production of high quality models with a limited effort in the study area, where sinkholes tend to cluster and form fault-controlled alignments (e.g. Galve et al., 2009b).

Acknowledgments

The authors would like to thank M.A. Moin, R. Meraji, M. Safari, H. Musivand and H. Vafaei (Hamadan Regional Water Authority) for supplying data and reports, as well as M. Keyvan nia, A.A. Moradnezhad, and F. Mohsenipour for their help in the field. We also acknowledge Dr. S. Pourdad, Dr. Isolina Alberto (University of Zaragoza) and the reviewers Dr. Mario Parise and Dr. J.P. Galve for useful suggestions, as well as Mrs. S. Namdari (Tabriz University) for valuable discussions and comments on

GIS, and the Research Committee of Kermanshah Regional Water Authority for their cooperation. The contribution by F. Gutiérrez has been supported by the Spanish national projects CGL2010-16775 and CGL2013-40867-P (Ministerio de Economía y Competitividad).

References

Amiri, M., 2005. The effect of bedrock dissolution and pumping on Hamadan sinkholes occurrences. In: Taheri, K. (Ed.), Proceedings of the Conference on Hazards of Sinkholes in Karst Terrains. Kermanshah, Iran, pp. 43–68 (in Farsi).

Aurit, M.D., Paterson, R.O., Blanford, J.I., 2013. A GIS analysis of the relationship between sinkholes, dry-well complaints and groundwater pumping for frost-freeze protection of winter strawberry production in Florida. PLoS ONE 8, 1–9.

Batayneh, A.T., 2006. Use of electrical resistivity methods for detecting subsurface fresh and saline water and delineating their interfacial configuration: a case study of the eastern Dead Sea coastal aquifers, Jordan. Hydrogeol. J. 14, 1277–1283.

Bednarik, M., Magulova, B., Matys, M., Marschalko, M., 2010. Landslide susceptibility assessment of the Kralovany–Liptovsky Mikulas railway case study. Phys. Chem. Earth 35, 162–171.

Bruno, E., Calcaterra, D., Parise, M., 2008. Development and morphometry of sinkholes in coastal plains of Apulia, southern Italy. Preliminary sinkhole susceptibility assessment. Eng. Geol. 99, 198–209.

Dogan, U., Yilmaz, M., 2011. Natural and induced sinkholes of the Obruk Plateau and Karapinar–Hotamis Plain, Turkey. J. Asian Earth Sci. 40, 496–508.

Donevska, K.R., Gorsevski, P.V., Jovanovski, M., Pes˘evski, I., 2012. Regional non-hazardous landfill site selection by integrating fuzzy logic, AHP and geographic information systems. Environ. Earth Sci. 67, 121–131.

Drever, J.I., 1997. The Geochemistry of Natural Waters: Surface and Groundwater Environments. Prentice Hall, New Jersey.

Dunham, R.J., 1962. Classification of carbonate rocks according to depositional texture. In: Ham, W.E. (Ed.), Classification of Carbonate Rocks. Memoir 1. American Association of Petroleum Geologists, pp. 108–121.

Dweiri, F., Al-Oqla, F.M., 2006. Material selection using analytical hierarchy process. Int. J. Comput. Appl. Technol. 26, 82–189.

Edmonds, C., Green, C., Higginbottom, I., 1987. Subsidence hazard prediction for limestone terrains as applied to the English Cretaceous chalk. Geol. Soc. Eng. Geol. Spec. Publ. 4, 283–293.

Falaschi, F., Giacomelli, F., Federici, P.R., Puccinelli, A., D'Amato, A.G., Pochini, A., Ribolini, A., 2009. Logistic regression versus artificial neural networks: landslide susceptibility evaluation in a sample area of the Serchio River valley, Italy. Nat. Hazards 50, 551–569.

Fidelibus, M.D., Gutiérrez, F., Spilotro, G., 2011. Human-induced hydrogeological changes and sinkholes in the coastal gypsum karst of Lesina Marina area (Foggia Province, Italy). Eng. Geol. 118, 1–19.

Galve, J.P., Bonachea, J., Remondo, J., Gutierrez, F., Guerrero, J., Lucha, P., Cendrero, A., Gutierrez, M., Sanchez, J.A., 2008. Development and validation of sinkhole susceptibility models in mantled karst settings, a case study from the Ebro valley evaporite karst (NE Spain). Eng. Geol. 99, 185–197.

Galve, J.P., Gutiérrez, F., Remondo, J., Bonachea, J., Lucha, P., Cendrero, A., 2009a. Evaluating and comparing methods of sinkhole susceptibility mapping in the Ebro Valley evaporite karst (NE Spain). Geomorphology 111, 160–172.

Galve, J., Gutiérrez, F., Lucha, P., Guerrero, J., Remondo, J., Bonachea, J., Cendrero, A., 2009b. Probabilistic sinkhole modelling for hazard assessment. Earth Surf. Process. Landf. 34, 437–452.

Galve, J.P., Gutiérrez, F., Lucha, P., Bonachea, J., Remondo, J., Cendrero, A., Gutiérrez, M., Gimeno, M.J., Pardo, G., Sánchez, J.A., 2009c. Sinkholes in the salt-bearing evaporite karst of the Ebro River valley upstream of Zaragoza city (NE Spain): geomorphological mapping and analysis as a basis for risk management. Geomorphology 108, 145–158.

Galve, J.P., Remondo, J., Gutiérrez, F., 2011. Improving sinkhole hazard models incorporating magnitude–frequency relationships and nearest neighbour analysis. Geomorphology 134, 157–170.

Galve, J.P., Gutiérrez, F., Guerrero, J., Alonso, J., Ignacio, D., 2012a. Optimizing the application of geogrids to roads in sinkhole-prone areas on the basis of hazard models and cost–benefit analyses. Geotext. Geomembr. 34, 80–92.

Galve, J.P., Gutiérrez, F., Guerrero, J., Alonso, J., Ignacio, D., 2012b. Application of risk, cost–benefit and acceptability analyses to identify the most appropriate geogrid solution to mitigate sinkhole damage on roads. Eng. Geol. 145–146, 65–77.

Gao, S., Hegg, D.A., Frick, G., Caffrey, P.F., Pasternack, L., Cantrell, C., Sullivan, W., Ambrusko, J., Albrechcinski, T., Kirchstetter, T.W., 2001. Experimental and modeling studies of secondary organic aerosol formation and some applications to the marine boundary layer. J. Geophys. Res. 106 (27), 619–634.

García-Moreno, I., Mateos, R.M., 2011. Sinkholes related to discontinuous dumping: susceptibility zapping based on geophysical Studies. The case of Cresttx (Mallorca, Spain). Environ. Earth Sci. 64, 523–537.

Geological and Mineral Survey of Iran, 1979. Quadrant Map of KabudarAhang. Scale 1: 250,000. Tehran, Iran.

Ghasemi, W., Talbot, A., 2006. A new tectonic scenario for the Sanandaj–Sirjan Zone (Iran). J. Asian Earth Sci. 26, 683–693.

Gunn, J. (Ed.), 2004. Encyclopedia of Caves and Karst Science. Fitzroy Dearborn, New York.

Gutiérrez, F., 2010. Hazards associated with karst. In: Alcántara, I., Goudie, A. (Eds.), Geomorphological Hazards and Disaster Prevention. Cambridge University Press, Cambridge, pp. 161–175.

Gutiérrez, F., Cooper, A., 2002. Evaporite dissolution subsidence in the historical city of Calatayud, Spain: damage appraisal and prevention. Nat. Hazards 25, 259–288.

Gutiérrez, F., Galve, J.P., Guerrero, J., Lucha, P., Cendrero, A., Remondo, J., Bonachea, J., Gutiérrez, M., Sánchez, J.A., 2007. The origin, typology, spatial distribution, and detrimental effects of the sinkholes developed in the alluvial evaporite karst of the Ebro River valley downstream Zaragoza city (NE Spain). Earth Surf. Process. Landf. 32, 912–928.

Gutiérrez, F., Cooper, A.H., Johnson, K.S., 2008a. Identification, prediction, and mitigation of sinkhole hazards in evaporite karst areas. Environ. Geol. 53, 1007–1022.

Gutiérrez, F., Guerrero, J., Lucha, P., 2008b. A genetic classification of sinkholes illustrated from evaporate paleokarst exposures in Spain. Environ. Geol. 53, 993–1006.

Gutiérrez, F., Parise, M., De Waele, J., Jourde, H., 2014. A review on natural and human-induced geohazards and impacts in karst. Earth Sci. Rev. 138, 61–88.

Heidari, M., Khanlari, G.R., Taleb Beydokhti, A.R., Momeni, A.A., 2011. The formation of cover collapse sinkholes in North of Hamedan, Iran. Geomorphology 132, 76–86.

Ho, W., 2008. Integrated analytic hierarchy process and its applications — a literature review. Eur. J. Oper. Res. 186, 211–228.

Jiang, X., Lei, M., Li, Y., Dai, J., 2005. National-scale risk assessment of sinkhole hazard in China. In: Beck, B.F. (Ed.), Sinkholes and the Engineering and Environmental Impacts of Karst. Proceedings of the Tenth Multidisciplinary Conference San Antonio, Texas, September 24 – 28, ASCE Geotechnical Special Publication, No. 144, pp. 649–658.

Karimi, H., Taheri, K., 2010. Hazards and mechanism of sinkholes on Kaboudar Ahang and Famenin plains of Hamadan, Iran. Nat. Hazards 55, 481–499.

Kaufmann, J.E., 2008. A statistical approach to karst collapse hazard analysis in Missouri. In: Yuhr, L.B., Calvin Alexander, E., Beck, B.F. (Eds.), Sinkholes and the Engineering and Environmental Impacts of Karst, 183. ASCE Geotechnical Special Publication, Huntsville, pp. 257–268.

Khanlari, G., Heidari, M., Momeni, A.A., Ahmadi, M., Taleb Beydokhti, A., 2012. The effect of groundwater overexploitation on land subsidence and sinkhole occurrences, western Iran. Q. J. Eng. Geol. Hydrogeol. 45, 447–456.

Langmuir, D., 1997. Aqueous Environmental Geochemistry. Prentice-Hall Inc., New Jersey.

Lindsey, B.D., Katz, B.G., Berndt, M.P., Ardis, A.F., Skach, K.A., 2010. Relations between sinkhole density and anthropogenic contaminants in selected carbonate aquifers in the eastern United States. Environ. Earth Sci. 60, 1073–1090.

Margiotta, S., Negri, S., Parise, M., Valloni, R., 2012. Mapping the susceptibility to sinkholes in coastal areas, based on stratigraphy, geomorphology and geophysics. Nat. Hazards 62, 657–676.

Milanović, P., 2004. Water Resources Engineering in Karst. CRC, Boca Raton.

Milanović, P., 2011. Dams and reservoirs in karst. In: Van Beynen, P.E. (Ed.), Karst Management. Springer, pp. 47–74.

Munier, N., 2011. A Strategy for Using Multicriteria Analysis in Decision-making; a Guide for Simple and Complex Environmental Projects. Springer, Chichester.

Newton, J.G., 1984. Sinkholes resulting from ground-water withdrawals in carbonate terranes-an overview. Rev. Eng. Geol. 6, 195–202.

Ouhadi, V.R., Bakhshalipour, H., 2010. Impact of nanoclays on the behavior properties of collapsible soils. 9th International Congress on Advances in Civil Engineering. Karadeniz Technical University, Trabzon, Turkey.

Ouhadi, V.R., Goodarzi, A.R., 2010. Impact of solubility of carbonate or sulfate salts and collapsible potential on the formation of sinkholes. Eng. J. Tabriz Univ. 34, 1–10 (in Farsi, with English Abstr.).

Papadopoulou-Vrynioti, K., Bathrellos, G.D., Skilodimou, H.D., Kaviris, G., Makropoulos, K., 2013. Karst collapse susceptibility mapping considering peak ground acceleration in a rapidly growing urban area. Eng. Geol. 158, 77–88.

Parise, M., 2012. A present risk from past activities: sinkhole occurrence above underground quarries. Carbonates Evaporites 27, 109–118.

Parise, M., 2013. Recognition of instability features in artificial cavities. In: Filippi, M., Bosak, P. (Eds.), Proceedings 16th International Congress of Speleology. Brno vol. 2, pp. 224–229.

Parise, M., Lollino, P., 2011. A preliminary analysis of failure mechanisms in karst and man-made underground caves in Southern Italy. Geomorphology 134, 132–143.

Pourghasemi, H.R., Pradhan, B., Gokceoglu, C., 2012. Application of fuzzy logic and analytical hierarchy process (AHP) to landslide susceptibility mapping at Haraz watershed, Iran. Nat. Hazards 63, 965–996.

Pourghasemi, H.R., Moradi, H.R., Fatemi Aghda, S.M., 2013. Landslide susceptibility mapping by binary logistic regression, analytical hierarchy process, and statistical index models and assessment of their performances. Nat. Hazards 69, 749–779.

Pueyo-Anchuela, O., Pocoví Juan, A., Soriano, M.A., Casas-Sainz, A.M., 2009. Characterization of karst hazards from the perspective of the doline triangle using GPR. Examples from Central Ebro Basin (Spain). Eng. Geol. 108, 225–236.

Saaty, T.L., 1977. A scaling method for priorities in hierarchical structures. J. Math. Psychol. 15, 234–281.

Saaty, T.L., 1980. Multicriteria Decision Making. The Analytic Hierarchy Process. McGraw-Hill, New York.

Saaty, T.L., 2001. Decision Making for Leaders. The Analytic Hierarchy Process for Decision in a Complex World New edition. RWS Publications, Pittsburgh.

Salvati, R., Sasowsky, I.D., 2002. Development of collapse sinkholes in areas of groundwater discharge. J. Hydrol. 264, 1–11.

Shalev, E., Lyakhovsky, V., 2012. Viscoelastic damage modeling of sinkhole formation. J. Struct. Geol. 42, 163–170.

Soffianian, A.R., Mohamadi Towfigh, E., Khodakarami, L., Amiri, F., 2011. Land use mapping using artificial neural network (case study: Kaboudarahang, Razan and Khonjin-Talkhab catchment in Hamedan province). J. Appl. RS GIS Tech. Nat. Resour. Sci. 2, 1–13.

Song, K.I., Cho, G.C., Chang, S.B., 2012. Identification, remediation, and analysis of karst sinkholes in the longest railroad tunnel in South Korea. Eng. Geol. 135–136, 92–105.

Sprynskyy, M., Labedynets, M., Sadurski, A., 2009. Gypsum karst intensification as a consequence of sulphur mining activity (Jaziv field, Western Ukraine). Environ. Geol. 57, 173–181.
Taheri, K., Hashemi, M., 2010. Kurdish karst literature and resources use in the Awramanat Karst lands of western Zagros. Proceeding of the International Conference and Field Seminar Asian Trans-Disciplinary Karst Conference Polydoor & Faculty of Geography GMU. ISBN: 978-602-8487-17-7, p. v, 471 2.5 cm.
Taheri, K., Hashemi, M., 2011. Kurdish karst literature and resources use in the Awramanat Karst lands of western Zagros, Iran. Asian Trans-Disciplinary Karst Conference (Yogyakarta, Indonesia).
Taheri, K., Parvizi, F., Valizadeh, R., 2005. An introduction to sinkholes of Hamadan. Cheshmeh-e Honar w Danesh Pub., Kermanshah, Iran (64 pp.).
Thanh, L.N., De Smedt, F., 2012. Application of an analytical hierarchical process approach for landslide susceptibility mapping in A Luoi district, Thua Thien Hue Province, Vietnam. Environ. Earth Sci. 66, 1739–1752.
Tharp, T.M., 1999. Mechanics of upward propagation of cover-collapse sinkholes. Eng. Geol. 52, 23–33.
Tharp, T.M., 2002. Poroelastic analysis of cover-collapse sinkhole formation by piezometric surface drawdown. Environ. Geol. 42, 447–456.
Tolmachev, V., Leonenko, M., 2011. Experience in collapse risk assessment of building on covered karst landscapes in Russia. In: Van Beynen, P. (Ed.), Karst Management. Springer, Berlin, pp. 75–102.
Tzeng, G.H., Huang, J.J., 2011. Multiple Attribute Decision Making, Methods and Applications. CRC Press, Taylor & Francis Group, Oxford.
Voogd, H., 1983. Multi-criteria Evaluations for Urban and Regional Planning. Pion, London.
Waltham, T., 2008. Sinkhole hazarsd case histories in karst terrains. Q. J. Eng. Geol. Hydrogeol. 41, 291–300.
Waltham, A.C., Fookes, P.G., 2003. Engineering classification of karst ground conditions. Q. J. Eng. Geol. Hydrogeol. 36, 101–118.
Waltham, T., Bell, F., Culshaw, M., 2005. Sinkholes and Subsidence. Karst and Cavernous Rocks in Engineering and Construction. Springer, Chichester.
White, W.B., 1988. Geomorphology and Hydrology of Karst Terrains. Oxford University Press, New York.
Yang, Y.Y., Xu, Y.S., Shen, S.L., Yuan, Y., Yin, Z.Y., 2015. Mining-induced geo-hazards with environmental protection measures in Yunnan, China: an overview. Bull. Eng. Geol. Environ. 74, 141–150.
Ying, X., Guang-Ming, Z., Gui-Qiu, C., Lin, T., Ke-Lin, W., Dao-You, H., 2007. Combining AHP with GIS in synthetic evaluation of eco-environment quality, a case study of Hunan Province, China. Ecol. Model. 209, 97–109.
Zamiran Consulting Engineers, 2003. Sinkholes and Subsidence Studies in Kabudar Ahang and Famenin Plains. West Regional water Authority, Kermanshah, Iran (Report).
Zhou, W., Beck, B.F., 2011. Engineering issues on karst. In: Van Beynen, P.E. (Ed.), Karst Management. Springer, pp. 9–45.